JOURNAL OF AIRCRAFT
Vol. 43, No. 6, November–December 2006

Trajectory Management Concepts for Future Small Aircraft Transportation Systems

Brett Newman,* Colin Britcher,† Yenew Kassaye,‡ John Roy,§ Michael Krizansky,‖ and Michael Acheson¶
Old Dominion University, Norfolk, Virginia 23529

DOI: 10.2514/1.20960

Methodology for construction and implementation of in-flight trajectory management systems for vehicles participating in future small aircraft transportation systems is considered. The small aircraft transportation systems concept is a modern regional airspace system exploiting integration of key airborne and ground infrastructure technologies to facilitate efficiency and safety improved operations at noncontrolled public-use airports. An area where new trajectory management guidance systems may provide significant benefit is the transition between en route flight and the terminal airspace boundary, or possibly interior terminal airspace navigation fix points, for both approach and departure. Energy state theory and space–time curve geometry are investigated as tools for tailoring time to interface or time to land with traffic constraints. Results imply the trajectory management concepts offer significant design freedom to tailor flight paths and vehicle states for optimum performance and safety in real time. This strategy will also tend to provide practical trajectory profiles while avoiding heavy computational burdens.

I. Introduction

THE goal of the National Aeronautics and Space Administration (NASA) Small Aircraft Transportation System [1] (SATS) program is to develop key airborne and ground infrastructure technologies to facilitate: 1) high-volume operations (HVO): simultaneous multi-aircraft operations in nonradar airspace around public-use nontowered airports in near all-weather, and 2) lower landing minima (LLM): precision arrivals and approach guidance to public-use airports without approach lighting or ground-based guidance. LLM, as defined for the SATS program, is concerned primarily with three-dimensional flight-path guidance during approach, missed approach, and departure phases while operating under HVO procedures and restrictions. Within the existing HVO framework [2–4] based on an alternating sequence, T-shaped approach strategy with waypoint navigation segments and multi-altitude circular holding patterns with missed approach and external entry allowances, little design freedom is available for exploiting high-performance trajectory management guidance. Standard guidance systems implementing predefined rectilinear approach and departure segments will suffice here [5].

Under the current HVO operational concept, an area where advanced trajectory management guidance systems may provide significant benefit is the transition between en route flight phases and HVO terminal airspace operations for both approach and departure objectives. In this transition regime, flight paths are relatively unrestricted, thus providing an opportunity to apply energy state management for approaches and/or departures with potentially significant design freedom to tailor flight trajectories and vehicle energies for optimal performance and safety in real time. Consider for example, a high-performance SATS aircraft approaching a mixed commercial/business/general aviation traffic terminal airspace environment from arbitrary direction and time with variable speed and altitude. After being assigned to the approach sequence, the vehicle would nominally implement a descent trajectory constrained by the sequence assignment and associated traffic. If, on the other hand, the SATS aircraft was assigned with a special sliding sequence or free-flight designation, the energy state of the SATS aircraft could be optimally managed to the required threshold value [circular holding pattern entry point for current HVO procedures, or intermediate/final approach fix (IAF/FAF) for relaxed HVO procedures], while simultaneously merging with other traffic. Resulting operations might represent a significant reduction in fuel burn (coordinated speed–altitude maneuvering), time (prioritized, direct trajectories), and noise (minimal throttle movement) while balancing risk to traffic conflicts (midair collisions) and undesirable atmospheric phenomena (energetic weather or turbulence). Associated motion will be described by spatially curved, temporally coordinated trajectories with variable heading, flight path, and speed variables.

Objectives of this investigation are to explore the basic feasibility and potential benefit from such a system by conducting preliminary engineering studies. Documentation of these efforts is described in Secs. II and III. Section II focuses on transition between en route flight and the terminal airspace boundary with subsections covering the general methodology for trajectory generation, a numerical example, and a cockpit display system that will assist pilots in manually flying the approach–departure trajectories. Section III addresses aspects of flight inside the terminal airspace with subsections describing the general trajectory construction methodology, two numerical examples, and a control system that can automatically fly the desired trajectories. In addition, Sec. IV provides a vision of a general, fully developed trajectory management guidance system applicable to future SATS environments in the areas of functionality and input–output structure. Additional research and development is required to fully realize this vision.

Presented at the 24th Digital Avionics Systems Conference, Arlington, Virginia, 30 October–3 November 2005; received 7 November 2005; revision received 23 April 2006; accepted for publication 25 April 2006.

*Associate Professor, Department of Aerospace Engineering. Associate Fellow AIAA.
†Professor and Chair, Department of Aerospace Engineering. Associate Fellow AIAA.
‡M.S. Graduate; currently Structural Analyst, Boeing Integrated Defense Systems, Mail Stop 6M6-31, Renton, WA 98055. Member AIAA.
§M.S. Graduate, currently Performance Analyst, Dynetics, P.O. Box 5500, Huntsville, AL 35814. Member AIAA.
‖M.S. Candidate, currently Airfoils Lead, General Electric Aviation, Princeton Hill, M/D-30, Cincinnati, OH 45246. Member AIAA.
¶M.S. Candidate, currently Safety Engineer, NASA Langley Research Center, Mail Stop 267, Hampton, VA 23681. Member AIAA.

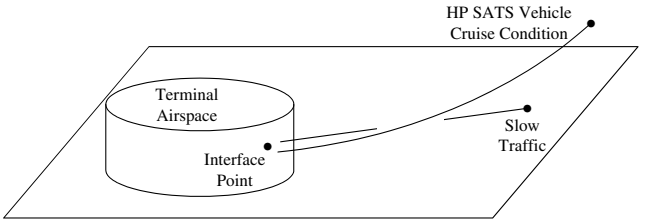

Fig. 1 Transition geometry.

II. Transition to SATS Airspace

The focus of this section is trajectory management for transition between en route flight conditions and terminal airspace operations located around a designated SATS airport. Emphasis is given to the arrival phase using manual flight, but concepts presented here could be extended to the departure phase as well. A quasi-optimal approach using energy state theory [6,7] to tailor time to interface at the terminal airspace boundary with consideration for traffic constraints is taken. Other performance objectives can be addressed with the same approach. This strategy will tend to provide simple, yet desirable, flight profiles while avoiding significant computational difficulties.

Figure 1 shows the descent of a generic high-performance SATS vehicle from cruise condition to the interface point at the terminal airspace boundary surrounding the SATS airport. Terminal airspace is of cylindrical shape with details described in Sec. III. Also shown is a slow-moving vehicle representing traffic flying to the same interface point. In this mixed aircraft environment, the high-performance vehicle may be held up by the slower traffic, resulting in airspace throughput inefficiencies and wasted time. Sought is a method to fly a managed variable curvilinear trajectory that is time-adjustable to circumvent the slow traffic at the interface point, or sequence behind the traffic, by exploiting SATS performance. Such a method is discussed next in the context of energy state theory, example results, and cockpit display system for manual piloting of the trajectories.

A. Energy State Trajectory

During ascent–descent flight, not only is attainment of the specified height of importance, but the associated speed as well. A single variable that incorporates both height and speed is energy height H_E, or [7]

$$H_E = H + \frac{1}{2}\frac{V^2}{g} \tag{1}$$

In Eq. (1), H denotes geometric height, V denotes total velocity (which equals true airspeed for zero wind), and g denotes gravity. Figure 2 shows a speed–altitude chart with contours of constant H_E that are independent of any vehicle. Energy height time rate of change $\dot{H}_E$ can be related to the longitudinal motion equation involving thrust T, drag D, and weight W, or

$$\dot{H}_E = \frac{(T-D)V}{W} = \dot{H} + \frac{V}{g}\dot{V} \tag{2}$$

Note $\dot{H}_E$ equals specific or weight normalized excess power $\mathcal{P}_E$. Figure 2 also shows contours of constant $\dot{H}_E$ for typical altitude-dependent thrust and parabolic drag polar represented as

$$\begin{aligned} T &= T_0(\Delta_{\text{Th}})\frac{\rho(H)}{\rho_0}, \qquad D = qS\left(C_{D_0} + kC_L^2\right) \\ C_L &= \frac{W}{q(H,V)S}, \qquad q = \tfrac{1}{2}\rho(H)V^2 \end{aligned} \tag{3}$$

In Eq. (3), ρ denotes atmospheric density, q denotes dynamic pressure, S denotes reference area, C_{D_0} denotes zero lift drag coefficient, C_L denotes lift coefficient, k denotes induced drag factor, Δ_{Th} denotes throttle input, and subscript 0 denotes sea level condition (T, ρ). Equation (3) also implies shallow ascents–descents.

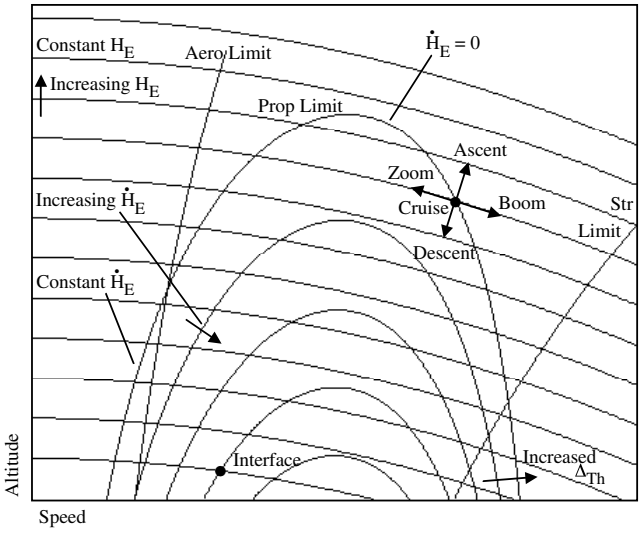

Fig. 2 H_E and $\dot{H}_E$ contours.

For a fixed Δ_{Th}, level flight or cruise equilibrium corresponds to points on the $\dot{H}_E = 0$ contour as indicated in Fig. 2. To perform a minimum time ascent, the vehicle would first execute a short-time zoom or conservative ascent by departing equilibrium with attack angle change to follow the curve of constant H_E to a tangency point between the H_E and $\dot{H}_E$ contours. The vehicle would then execute a regular or dissipative ascent following the tangency points until specific excess power [climb rate and acceleration, see Eq. (2)] is reduced to zero. In Fig. 2, ascent is limited by propulsion factors, not aerodynamics. In contrast, to perform a minimum time descent, the vehicle first executes a short-time boom or conservative descent following the constant H_E curve until minimum ($\dot{H}_E < 0$, not shown) $\dot{H}_E$ is typically achieved at the structural limit. The vehicle then follows the limit down to sea level, executing a regular or dissipative descent.

Minimum time ascent–descent profiles discussed previously are idealistic cases and somewhat impractical for SATS. Furthermore, minimum time performance may not be required. Trajectory management logic that facilitates adjustable flight time as a design parameter but still uses the graphical framework of Fig. 2 is more applicable for SATS. Such logic is considered next.

Practical timed descents from cruise to the terminal airspace interface point can be achieved by reducing and refixing Δ_{Th} and

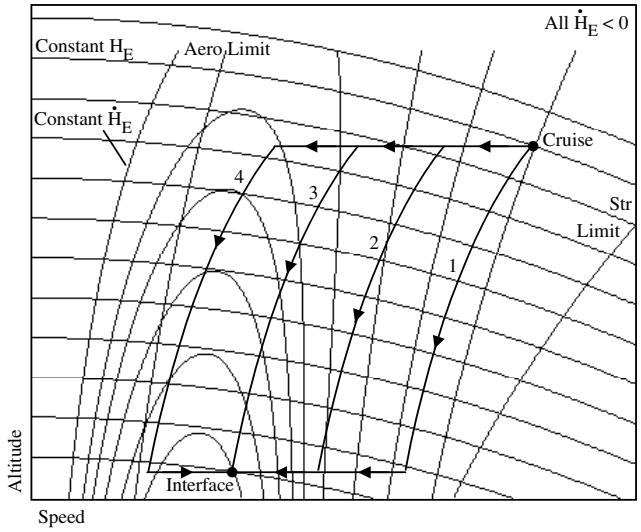

Fig. 3 H_E and $\dot{H}_E$ descent profiles.

adjusting descent attack angle for desired characteristics. Note in Fig. 2 that when Δ_{Th} is reduced, a new family of $\dot{H}_E$ contours result and the original cruise point with $\dot{H}_E = 0$ instantaneously converts to a $\dot{H}_E < 0$ point. At this new condition, the aircraft will inherently undergo descent, deceleration, or a combination thereof [see Eq. (2)]. Figure 3 depicts the speed–altitude chart after throttleback. Initial and final descent states (cruise and interface points, Fig. 2) are noted in Fig. 3 and several potential descent profiles are shown. Profile 1 is an immediate decelerating descent to the interface altitude followed by a pure deceleration segment to the interface speed. Profile 2 incorporates a pure deceleration segment at the beginning of Profile 1. Profile 3 extends the initial deceleration segment so that the descent arrives at the proper interface speed. Profile 4 extends the initial deceleration segment beyond profile 3, requiring pure acceleration after the descent to match the desired interface speed. Additional profiles that descend below interface altitude requiring short ending ascents are also possible. Although pure deceleration phases will most likely be short-time segments, the various profile characteristics can be used to adjust time to interface and to circumvent or comply with slower traffic approaching the interface point.

Descent type and initiation are two important factors for the trajectory management logic. Of interest here are constant q (or constant equivalent airspeed) descents that exhibit practical characteristics suitable for SATS. Equilibrium attack angle is scheduled with H according to Eq. (3) so that V accommodates a changing ρ value for specified q. Time to interface can be predicted by integrating velocities along the descent–deceleration profiles in Fig. 3. Note cruise segments at either the initial or final descent states must also be included in total flight time computation to yield proper ground distance. These pre- and post-cruise segments will be determined by the Δ_{Th} descent initiation time and can be used to adjust time to interface and to perform traffic resolution. The decelerating descent and pre-/post-cruise phases will likely be the largest contributors to flight time. Within this context, [8] explores alternative descent profiles computed from formal optimization.

B. Results

To demonstrate several en-route-to-terminal-airspace descent profiles, a flight performance model of a generic advanced 10-passenger light business jet commonly discussed in the SATS arena is considered. The vehicle is a point mass model described by Eq. (3) and

$$k = \frac{k_{\text{wing}}}{\pi A}, \qquad A = \frac{b^2}{S}, \qquad T_0 = T_{\max}\Delta_{\text{Th}} \tag{4}$$

In Eq. (4), k_{wing} denotes the wing induced drag factor, A denotes aspect ratio, b denotes span, $T_{\max}$ denotes maximum sea level thrust, and $0 \le \Delta_{\text{Th}} \le 1$. Numerical data for the parameters in Eqs. (3) and (4) include

$$\begin{gathered} S = 16.2\ \text{m}^2, \qquad b = 13.4\ \text{m}, \qquad W = 26,000\ \text{N} \\ C_{D_0} = 0.0231, \qquad k_{\text{wing}} = 1.25, \qquad T_{\max} = 10,700\ \text{N} \\ C_{L_{\max}} = 1.37 \quad \text{at } V = 43.7\ \text{m/s} \quad \text{and} \quad H = 0\ \text{m} \end{gathered} \tag{5}$$

Figures 4–8 show time, distance, speed, descent rate, and flight-path characteristics for three descent profiles similar to profiles 1–2 in Fig. 3. Conditions at cruise correspond to $H = 10,700$ m, $V = 175$ m/s, $\Delta_{\text{Th}} = 0.734$, and the interface point (runway threshold) is specified as $H = 42$ m and $V = 1.2(43.7)$ m/s. In each profile, the decelerating decent is executed with constant equivalent airspeed V_E. Each profile has a unique V_E described by the ratio of V_E with the cruise V_E. Speed ratios of 1, 0.9, and 0.8 are used. Each profile also has a unique time when the throttle is retarded, which is determined by the corresponding ground distance approximately matching the runway distance. A common throttle setting of $\Delta_{\text{Th}} = 0.05$ is used across all profiles. A small pure deceleration segment is applied at the end of each profile to match the desired 1.2 stall speed.

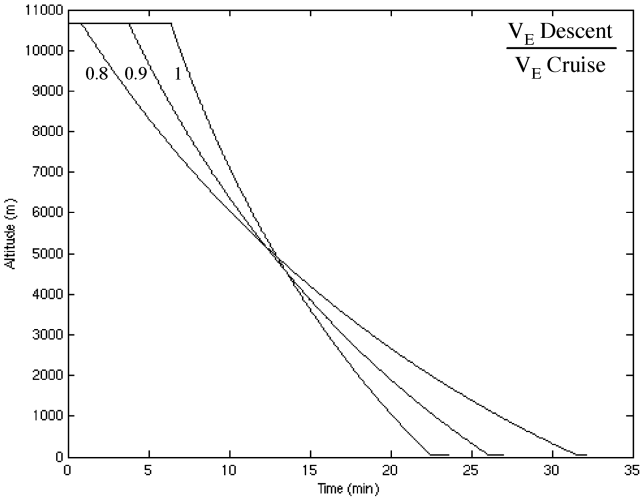

Fig. 4 Time profile.

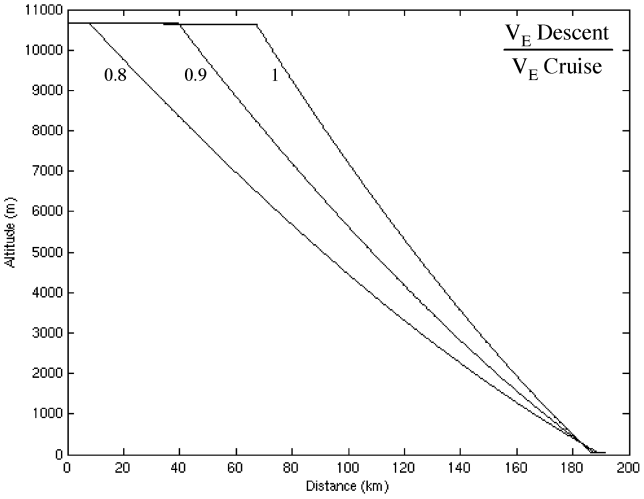

Fig. 5 Distance profile.

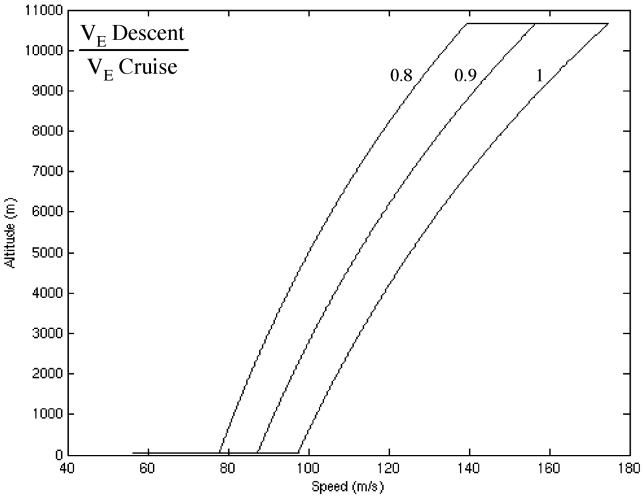

Fig. 6 Speed profile.

The key results and conclusions from Figs. 4–8 may be summarized as follows. Starting from the same initial cruise conditions, a SATS aircraft attempting to minimize time to interface and/or time to threshold would stay at cruise conditions as long as possible (the horizontal segment at top left of Figs. 4 and 5). A steep,

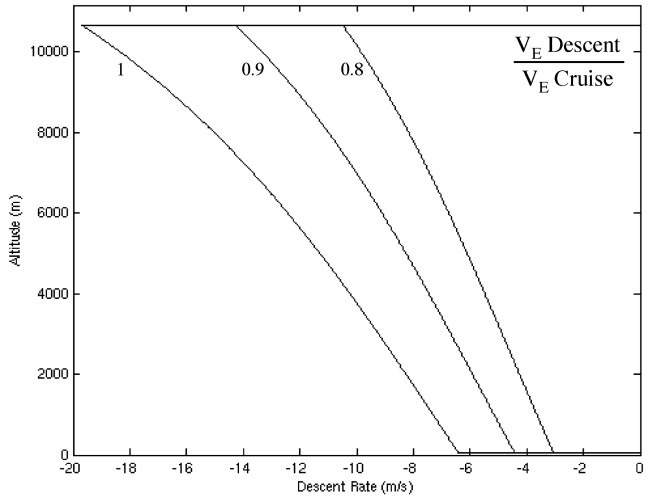

Fig. 7 Descent rate profile.

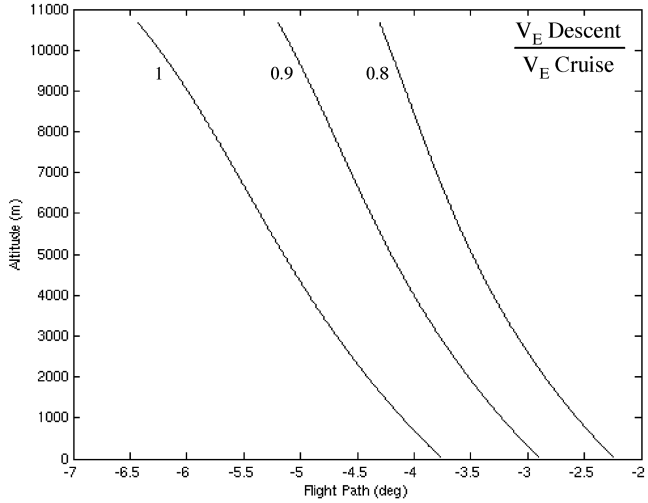

Fig. 8 Flight-path profile.

high-speed descent follows, shedding aircraft total energy at the maximum practical rate (structural, descent angle, V_{NE}, or similar limits in play). A flare is conducted at low altitude, followed by deceleration in approximately level flight or along a shallow glide slope. Had a longer time to interface and/or time to threshold been desired, the SATS aircraft would have broken from cruise *earlier* in time and *further* from the destination, following a shallower descent profile at a lower airspeed. It is found, in this example case, that substantial differences in arrival time at interface and/or threshold can be achieved with relatively small differences in choice of descent airspeed. Notable, however, is the fact that the descent profile must be decided at great distances from the destination, of the order of 160 km (100 miles) in this case. It must be emphasized that all descents are conducted at the same, constant, throttle setting ($\Delta_{Th} = 0.05$ here). The slower descent profiles are therefore expected to result in fuel savings compared with alternatives with similar elapsed times.

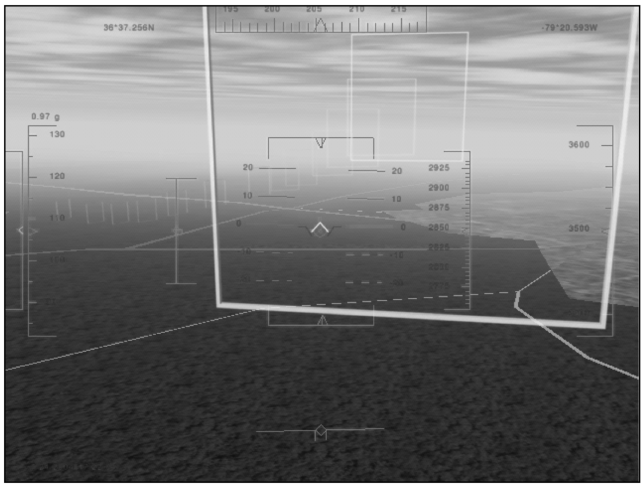

Fig. 9 Trajectory management display cues.

C. Energy State Display for Manual Piloting

Within a desktop simulator environment, [9] is exploring development of an advanced cockpit display interface system providing visual and numeric trajectory management data to assist human piloting of energy state descent profiles from Sec. II.A in a manual flight mode. Emphasis is being given to head-up displays that depict current and projected energy states, attitude and trajectory flight data, guidance and navigation cues, active constraint and envelope boundaries, traffic and weather conflicts, and system status and mode selection. The display will primarily show a real-time, three-dimensional trajectory corridor with markers indicating recommended flight tracks. Figure 9 illustrates some of the display concepts under study. Reference [9] is also exploring benefits of such a display system in reducing anxiety experienced by pilots when flight training transitions from visual meteorological conditions to instrument meteorological conditions, by affording these pilots a visual simulation of the intended flight path in three-dimensional space. The hypothesis is simulated exposure to the situation awareness will increase the comfort of the subject in future flight training, increase the attention to training detail, and thus increase the value of training time and expense.

III. Operation in SATS Airspace

The focus of this section is trajectory management for operations between entry–exit interface and runway threshold within terminal airspace located around a designated SATS airport. Emphasis is given to the landing phase using autoflight, but concepts presented here could be extended to the takeoff phase as well. A geometric approach using space–time curve theory [10] to tailor time to land with consideration for traffic constraints is taken. Other performance objectives can be addressed with similar approaches. This strategy will also tend to provide simple, yet desirable, flight profiles while avoiding significant computational difficulties.

Figure 10 is an approximate representation of HVO concept operations inside terminal airspace surrounding Danville Regional (KDAN) in southern Virginia. Terminal airspace is of cylindrical shape with 10 n mile radius (R in Fig. 10), 3000 ft ceiling, and offset from the intersection point of runways 02–13, which serves as the origin of a local east–north–up reference frame. Approach procedures for runway 02 are based on an alternating sequence, T-shaped approach path with waypoint navigation segments and multilayered holding patterns. Based on HVO rules and current traffic states [3,4], aircraft enter the holding patterns, and then proceed to the first, second, and third position fixes and, finally, runway threshold along predefined segments at specified speeds. It is important to emphasize the terminal airspace is a self-controlled area where the pilot flies according to HVO procedural rules, sequence assignment, and traffic state, with all associated data autonomously managed at a centralized ground station, rather than under the direction of a traditional human air controller located in an active tower [3,4]. Variables in Fig. 10 include length L, heading χ, and flight path Γ. Although this concept provides improved throughput efficiencies, the mixed aircraft environment may result in high-performance vehicles being held up by slower traffic. For vehicles with significant performance and accurate navigation knowledge of all airspace vehicles, a method to fly a managed variable curvilinear trajectory that is time adjustable to circumvent the slow traffic is sought. Such a method is discussed next in the context of geometric state theory, example results, and control system for autopiloting of the trajectories.

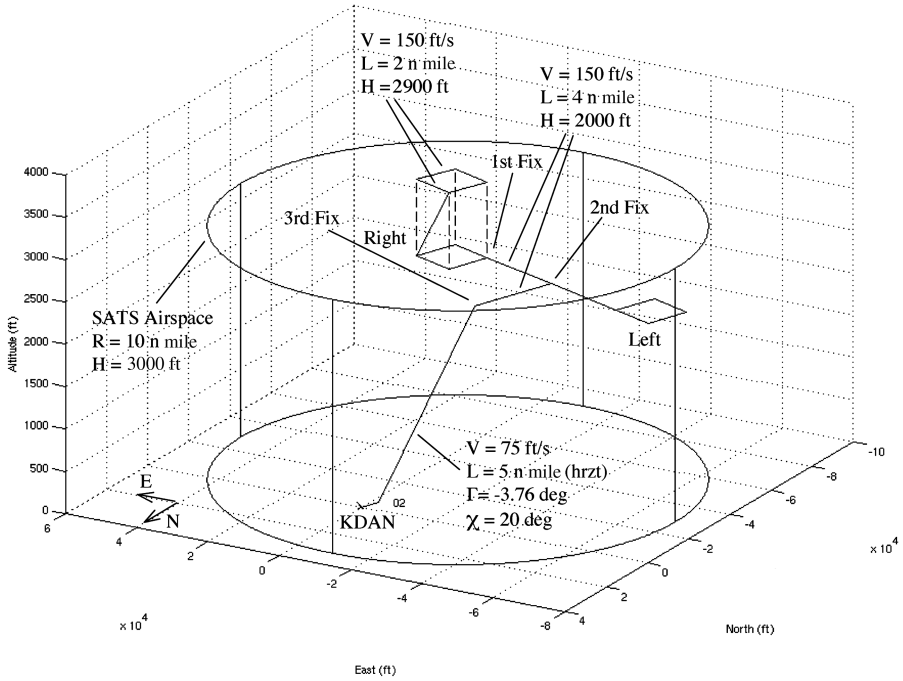

Fig. 10 Airspace geometry and regulations.

A. Geometric State Trajectory

Trajectory characteristics at the entry interface point on the terminal airspace boundary are fully described by vehicle position and velocity vectors $\boldsymbol{R}$ and $\boldsymbol{V}$ evaluated at the corresponding independent variable. Here the trajectory is parameterized by generic curve distance s. Trajectory characteristics at any suitable point that will yield desired runway threshold conditions also can be defined by appropriate $\boldsymbol{R}$ and $\boldsymbol{V}$. With the two specified conditions, trajectory management involves fitting an acceptable three-dimensional space curve to the boundary conditions. An infinite number of continuous functions can be fitted to the boundary points. When cast as an optimal path problem, a unique function can be constructed, often at great computational effort [11]. An alternative strategy more suited to real-time in-flight applications is to specify the function type, leaving only the function parameters as unknowns.

A specified path is described mathematically as [10]

$$\begin{aligned}\boldsymbol{R}(s) &= X(s, p_1, \ldots)\hat{\boldsymbol{I}} + Y(s, q_1, \ldots)\hat{\boldsymbol{J}} + Z(s, r_1, \ldots)\hat{\boldsymbol{K}}\\ \boldsymbol{R}'(s) &= X'(s, p_1, \ldots)\hat{\boldsymbol{I}} + Y'(s, q_1, \ldots)\hat{\boldsymbol{J}} + Z'(s, r_1, \ldots)\hat{\boldsymbol{K}}\end{aligned} \tag{6}$$

In Eq. (6), X, Y, and Z denote specified functions that depend on s and unknown parameters p_i, q_i, and r_i. Superscript $'$ denotes derivative with respect to s; hence, $\boldsymbol{R}'$ is a normalized velocity with unit magnitude or $\boldsymbol{V} = \dot{s}\boldsymbol{R}'$. X, Y, and Z also represent the fixed frame of reference with associated unit vectors $\hat{\boldsymbol{I}}$, $\hat{\boldsymbol{J}}$, and $\hat{\boldsymbol{K}}$. Specified boundary conditions at entry interface 1 and runway threshold 2 are expressed as

$$\boldsymbol{R}(s_i) = X_i\hat{\boldsymbol{I}} + Y_i\hat{\boldsymbol{J}} + Z_i\hat{\boldsymbol{K}}, \qquad \boldsymbol{R}'(s_i) = X_i'\hat{\boldsymbol{I}} + Y_i'\hat{\boldsymbol{J}} + Z_i'\hat{\boldsymbol{K}} \qquad i = 1, 2 \tag{7}$$

With Eqs. (6) and (7), the first task is to compute the unknown parameters p_i, q_i, and r_i, which fit the boundary conditions from

$$\begin{aligned} X_i &= X(s_i, p_1, \ldots), \qquad & X_i' &= X'(s_i, p_1, \ldots)\\ Y_i &= Y(s_i, q_1, \ldots), \qquad & Y_i' &= Y'(s_i, q_1, \ldots)\\ Z_i &= Z(s_i, r_1, \ldots), \qquad & Z_i' &= Z'(s_i, r_1, \ldots), \qquad i = 1, 2\end{aligned} \tag{8}$$

Equation (8) represents 12 nonlinear algebraic conditions. In cases where more than 12 parameters exist, excess parameters can be specified or intermediate trajectory points can be assigned. If no solution exists to Eq. (8), alternative X, Y, and Z functions must be considered.

Functions X, Y, and Z only describe the path spatially. The second task is to calibrate the path temporally. Generic curve speed $\dot{s}$ is specified functionally as

$$\dot{s} = f(s, g_1, \ldots) \tag{9}$$

In Eq. (9), f denotes the specified speed function that depends on s and specified parameters g_i. Function f and parameters g_i must accommodate the desired boundary conditions for speed at entry interface and runway threshold, or

$$f(s_i, g_1, \ldots) = \dot{s}_i, \qquad i = 1, 2 \tag{10}$$

Equation (9) is rewritten in differential form and integrated to obtain time t at any point along the trajectory corresponding to generic distance s.

$$\mathrm{d}t = \frac{1}{f(s, g_1, \ldots)}\mathrm{d}s, \qquad t - t_1 = \int_{s_1}^{s} \frac{1}{f(s, g_1, \ldots)}\mathrm{d}s$$
$$t_2 - t_1 = \int_{s_1}^{s_2} \frac{1}{f(s, g_1, \ldots)}\mathrm{d}s \tag{11}$$

Equation (11) also gives the expression for runway threshold time t_2. Time computation is performed analytically (when tractable) or numerically (otherwise).

Practical constraints imposed on the trajectory curve, such as maximum acceptable curvature and torsion values or minimum acceptable line-of-sight distance to traffic, will be necessary for safety reasons and general acceptance. Curvature κ_ρ and torsion κ_τ are defined as [10]

$$\kappa_\rho = |\hat{\boldsymbol{u}}'|, \qquad \kappa_\tau = |\hat{\boldsymbol{b}}'|, \qquad \hat{\boldsymbol{u}} = \boldsymbol{R}', \qquad \hat{\boldsymbol{n}} = \tfrac{1}{\kappa_\rho}\hat{\boldsymbol{u}}'$$
$$\hat{\boldsymbol{b}} = \hat{\boldsymbol{u}} \times \hat{\boldsymbol{n}} \tag{12}$$

Further, line of sight to traffic is defined as

$$R_{\text{los}} = |\boldsymbol{R}_T - \boldsymbol{R}| \tag{13}$$

where $\boldsymbol{R}_T$ denotes traffic position vector. With these definitions, trajectory inequality constraints appear as

$$\kappa_\rho \le \kappa_\rho^*, \qquad \kappa_\tau \le \kappa_\tau^*, \qquad R_{\text{los}}^* \le R_{\text{los}} \tag{14}$$

where superscript * denotes constraint value. When computing unknown parameters p_i, q_i, and r_i in Eq. (8), satisfaction of Eq. (14) across all times is required. Various computational methodologies can be applied here. In some situations, HVO traffic states will simply not allow feasible solutions to the trajectory management logic. No theoretical result is available to guarantee solution existence. However, by searching a finite but versatile set of specified function types, the trajectory management strategy can easily identify when lack of solution existence occurs. In such cases, the vehicle must follow standard HVO operations.

To implement the strategy outlined in this section, trajectory prediction of traffic is necessary. If traffic is of the standard SATS type, which follows known HVO procedures and intent, future traffic states are known and path prediction is realizable. If traffic is of the high-performance SATS type with free-flight designation, and assuming all vehicles in this class use common trajectory management systems, then their future state is also computable. No other traffic types are allowed in the terminal airspace under HVO. Note if two or more high-performance class vehicles are operating in free flight, nominal trajectory computations can be used to prioritize their arrival–departure sequence. All trajectories can be updated periodically through the available SATS air-to-air and air-to-ground communication links. With the traffic line-of-sight constraint, collision avoidance is guaranteed. If the trajectory management system somehow fails to predict a traffic conflict, baseline HVO procedures use a built-in conflict detection, alerting, and resolution (CDAR) system for a final layer of safety, similar to the traffic alert and collision avoidance system (TCAS) in common use.

B. Results

Figure 11 shows a right-turn scenario to runway 02 KDAN involving a high-performance (HP) SATS vehicle and slower traffic. Traffic 1 is located at the initial point on the downwind leg of the right holding track, and traffic 2 is located on the initial point of the upwind leg of the left holding track. Traffic movement conforms to the HVO rules in Fig. 10. HP SATS is approaching the airspace lined up with, but above, the T approach path located 6 n mile horizontally from fix 1 with flight conditions $H = 3000$ ft, $V = 250$ ft/s, $\Gamma = 0$ deg, and $\chi = 290$ deg.

Two candidate trajectories are shown in Fig. 11 for HP SATS. The standard trajectory conforms to HVO rules. In this case, HP SATS reduces speed and altitude (linear variation) to enter the upper right holding track designated third in the landing sequence. Traffic 1 approaches fix 2 first, turns for fix 3, and descends to land. While traffic 1 is approaching fix 2 and making the right turn, traffic 2 makes an extra circuit of the holding track. During this same period, HP SATS descends to the lower right holding track on the outward bound crosswind leg. As traffic 2 executes a left turn at fix 2 for fix 3, HP SATS has not yet reached fix 1. Following HVO operations, HP SATS makes an extra circuit of the holding track before descending to land.

The managed trajectory maintains altitude and speed into the airspace along a rectilinear path and then executes a curvilinear transition between a point directly above fix 1 and the fix 3 point with conditions $H = 2000$ ft, $V = 125$ ft/s, $\Gamma = -3.76$ deg, and $\chi = 20$ deg. HP SATS overflies and splits the traffic along this managed trajectory. The curvilinear segment is specified as a combination of elementary functions, specifically, a helix obtained from a circle (horizontal coordinates) and a hyperbola (vertical coordinate). The XYZ frame origin is located at the runway end point with Y along the runway direction, X pointing to the right of the runway direction, and Z directed up.

The hyperbola geometric center is located at $(X_{\text{hc}}, Y_{\text{hc}}, Z_{\text{hc}})$ and a local xyz reference frame is constructed at this point parallel to XYZ. The hyperbolic path is described in this local frame by

$$-\frac{y^2}{a^2} + \frac{z^2}{b^2} = 1, \qquad x = 0 \tag{15}$$

Unknown function parameters include X_{hc}, Y_{hc}, Z_{hc}, a, and b, and their computation is accomplished with local frame coordinates using y as the generic curve distance. Boundary conditions from Fig. 11 include

$$y_1 = 0, \qquad z_1 = -b, \qquad \frac{\mathrm{d}z}{\mathrm{d}y_1} = 0, \qquad y_2 = 4 \text{ n mile}$$
$$z_2 = -b - 1000 \text{ ft}, \qquad \frac{\mathrm{d}z}{\mathrm{d}y_2} = -\frac{2000 \text{ ft}}{5 \text{ n mile}} \tag{16}$$

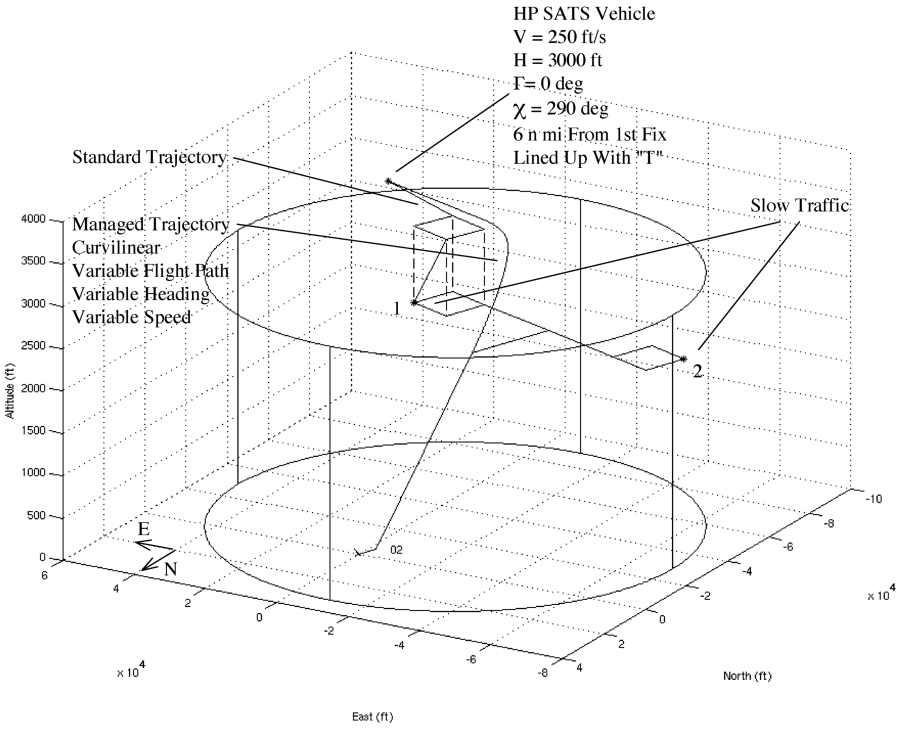

Fig. 11 Right-turn trajectory management; unconstrained case.

Application of the Eq. (16) boundary conditions to the Eq. (15) hyperbolic path yields the spatial solution:

$$X_{hc} = 0, \qquad Y_{hc} = -9 \text{ n mile}, \qquad Z_{hc} = b + 3000 \text{ ft}$$
$$b = -(z_1 - z_2)\frac{(z_1 - z_2) + \sigma_2 y_2}{2(z_1 - z_2) + \sigma_2 y_2} \qquad \left(\sigma = \frac{dz}{dy}\right) \tag{17}$$
$$a^2 = -\frac{b^2 y_2}{\sigma_2(b + z_1 - z_2)}$$

The circle geometric center is located at (X_{cc}, Y_{cc}, Z_{cc}) and a local xyz reference frame is constructed at this point parallel to XYZ. The circular path is described in this local frame by

$$x^2 + y^2 = r^2, \qquad z = 0 \tag{18}$$

Unknown function parameters include X_{cc}, Y_{cc}, Z_{cc}, and r, and although their values can be had by inspection, the formal process is summarized. Computation of the unknowns is accomplished with local frame coordinates using y as the generic curve distance. Note this is the same value used in hyperbolic path construction. Boundary conditions from Fig. 11 include

$$x_1 = 0, \qquad y_1 = -4 \text{ n mile}, \qquad \frac{dx}{dy_1} = -\infty$$
$$x_2 = -4 \text{ n mile}, \qquad y_2 = 0, \qquad \frac{dx}{dy_2} = 0 \tag{19}$$

Application of the Eq. (19) boundary conditions to the Eq. (18) circular path yields the spatial solution:

$$X_{cc} = 4 \text{ n mile}, \qquad Y_{cc} = -5 \text{ n mile}, \qquad Z_{cc} = 3000 \text{ ft}$$
$$r = -y_1 = -x_2 \tag{20}$$

The helical trajectory is obtained by combining the x and y coordinates from the circle with the z coordinate from the hyperbola.

Time calibration of the trajectory is accomplished with the specified speed function:

$$V = V_1 + (V_2 - V_1)\frac{z - z_1}{z_2 - z_1} \tag{21}$$

In Eq. (21), z is used as the generic curve distance. Note speed varies linearly with altitude. Integrating Eq. (21) horizontally yields the temporal solution:

$$t_2 - t_1 = \int_{y_1}^{y_2} \frac{1}{V\cos(\Gamma)}\,dy \tag{22}$$

with

$$\cos(\Gamma) = \frac{1}{[1 + (b^2/a^4)y^2[1 + (y^2/a^2)]^{-1}]^{1/2}} \tag{23}$$

Note Eq. (22) is integrated on y, implying Eq. (15) is used for substitution of z.

The standard trajectory requires a time of 1359.20 s for HP SATS to land. On the other hand, the managed trajectory only requires 571.18 s for HP SATS to land. A difference of 13.73 min in time to land exists between the two trajectories. The managed trajectory exploits the vehicle flight performance and accurate navigation knowledge of all airspace vehicles in the SATS concept to achieve a significant time savings. A similar straight-in scenario to runway 02 KDAN can be found in [12].

The right-turn scenario of Fig. 11 just considered is an unconstrained case. No restrictions were imposed on the line-of-sight distance to traffic as the descent trajectory was computed. A traffic line-of-sight constrained case is investigated next. Reconsider the right-turn scenario to runway 02 KDAN with identical flight and boundary conditions for HP SATS as in Fig. 11. However, consider a different traffic condition. In this case, slower traffic consists of a single vehicle (traffic) located at the initial point on the inward bound

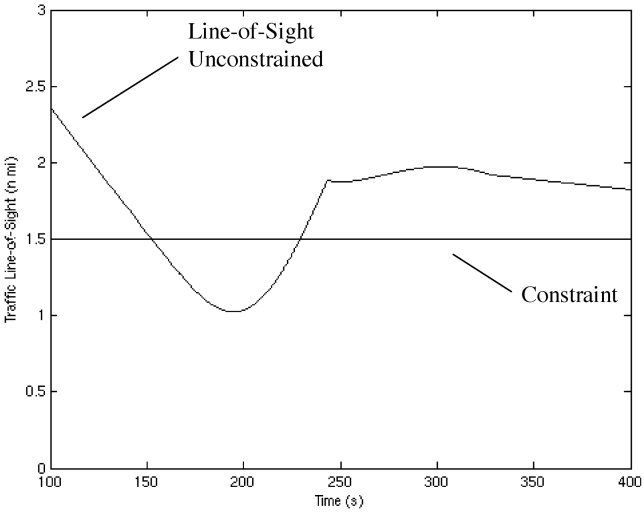

Fig. 12 Line-of-sight response; unconstrained case.

crosswind leg of the right holding track. Traffic proceeds through fix 1, fix 2 with a right turn, and fix 3, followed by a descent to land according to established HVO procedures. Simultaneously, HP SATS is to overfly traffic along some managed trajectory similar to that in Fig. 11, which also satisfies the line of sight to traffic constraint noted in Eq. (14).

One computational strategy for constructing a modified trajectory is to smoothly distort the associated unconstrained trajectory in a direction such that the relevant constraint is satisfied. Therefore, reconsider the unconstrained managed trajectory previously computed with elementary functions and depicted in Fig. 11. Figure 12 shows the corresponding traffic R_{los} behavior during this descent. As HP SATS approaches and overtakes traffic, R_{los} decreases, reaches a minimum of 1.02 n mile near 195 s, and then increases. As the final approach speed of HP SATS decreases below that of traffic, R_{los} attains a maximum of 1.97 n mile near 282 s and then gradually drops off. The sharp corner at 243 s corresponds to the traffic right turn at fix 2. For safety considerations, maintenance of a minimum line of sight $R^*_{los} = 1.5$ n mile is sought.

The initial step of the constraint calculation is determination of the minimum line-of-sight condition over the unconstrained trajectory.

$$t_{min} = t: \min_{t_1 \le t \le t_2} \{|\boldsymbol{R}_T(t) - \boldsymbol{R}(t)|\}, \qquad \boldsymbol{R}_{los_{min}} = \boldsymbol{R}_T(t_{min}) - \boldsymbol{R}(t_{min})$$
$$R_{los_{min}} = |\boldsymbol{R}_{los_{min}}| \tag{24}$$

For the final step, the HP SATS constrained position vector $\boldsymbol{R}_c$, which just satisfies the line-of-sight constraint, is computed by distorting the unconstrained position vector $\boldsymbol{R}$.

$$\boldsymbol{R}_c(t) = \boldsymbol{R}(t) - (\delta - 1)\phi(t)\boldsymbol{R}_{los_{min}}, \qquad \delta = \frac{R^*_{los}}{R_{los_{min}}} \qquad (1 < \delta)$$

$$\phi(t) = \begin{cases} 0 & \text{for } t_1 \le t \le t_{min} - \Delta t_- \quad (0 < \Delta t_- \le t_{min} - t_1) \\ \psi(t) & \text{for } t_{min} - \Delta t_- \le t \le t_{min} + \Delta t_+ \\ 0 & \text{for } t_{min} + \Delta t_+ \le t \le t_2 \quad (0 < \Delta t_+ \le t_2 - t_{min}) \end{cases}$$

$$\left(\psi(t), \frac{d\psi(t)}{dt}\right) = \begin{cases} (0,0) & \text{at } t = t_{min} - \Delta t_- \\ (1,0) & \text{at } t = t_{min} \\ (0,0) & \text{at } t = t_{min} + \Delta t_+ \end{cases} \tag{25}$$

In Eq. (25), the term $(\delta - 1)\phi(t)\boldsymbol{R}_{los_{min}}$ is used to smoothly distort the unconstrained trajectory. The distortion is in the $-\boldsymbol{R}_{los_{min}}$ direction and occurs over the time window $t_{min} - \Delta t_- \le t \le t_{min} + \Delta t_+$ where parameters Δt_- and Δt_+ are computed. Variable δ provides the proper amplitude to satisfy the constraint at t_{min} and function $\phi(t)$

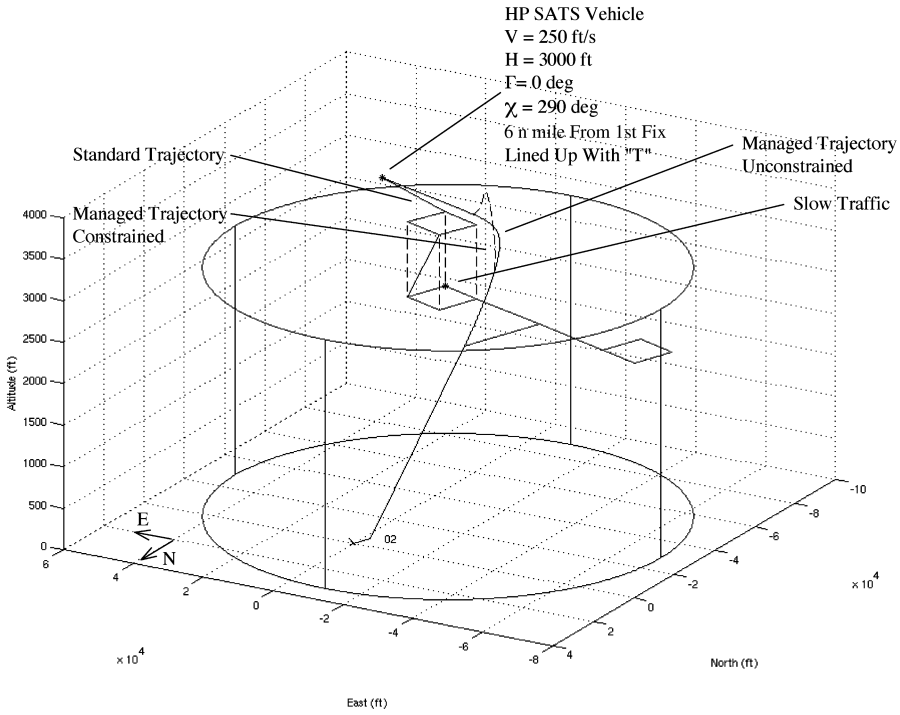

Fig. 13 Right-turn trajectory management; constrained case; perspective view.

[through $\psi(t)$] provides the distortion smoothness. Function $\psi(t)$ is any specified C^1 (continuous through first derivative) function meeting the exterior and interior conditions in Eq. (25). Here, $\psi(t)$ is specified using the sine function.

$$\psi(t) = 1/2[1 + \sin\{\omega[t - (t_{\min} - \Delta t_-)] - \pi/2\}], \qquad \omega = 2\pi/T$$
$$T = \Delta t_- + \Delta t_+, \qquad \Delta t_- = \Delta t_+ \tag{26}$$

At the component level, Eq. (25) is

$$X_c(t) = X(t) - (\delta - 1)\phi(t)X_{\text{los}_{\min}},$$
$$Y_c(t) = Y(t) - (\delta - 1)\phi(t)Y_{\text{los}_{\min}}, \tag{27}$$
$$Z_c(t) = Z(t) - (\delta - 1)\phi(t)Z_{\text{los}_{\min}}$$

With $R^*_{\text{los}} = 1.5$ n mile and $\Delta t_- = \Delta t_+ = 60$ s, Figs. 13–15 show the constrained trajectory overlaid on the unconstrained trajectory using perspective, side, and top views of the three-dimensional scenario. Note how the new trajectory has been smoothly distorted away from traffic in the critical region. The trajectory incorporates a mild ±500 ft altitude swell and gradual right–left S turn along the curvilinear descent trajectory. Figure 16 shows the corresponding traffic R_{los} behavior overlaid on the unconstrained result. Observe

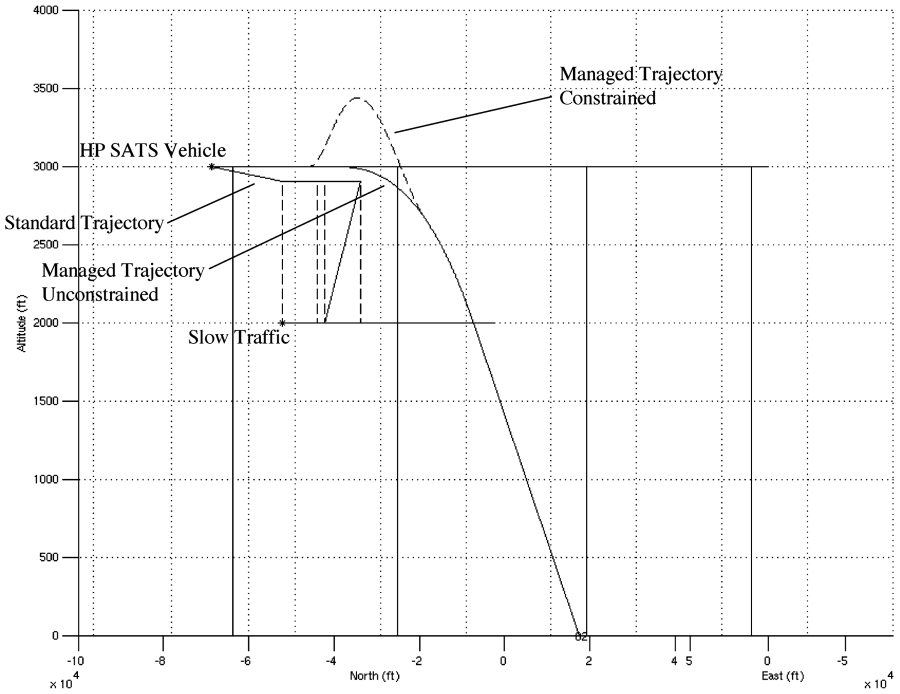

Fig. 14 Right-turn trajectory management; constrained case; side view.

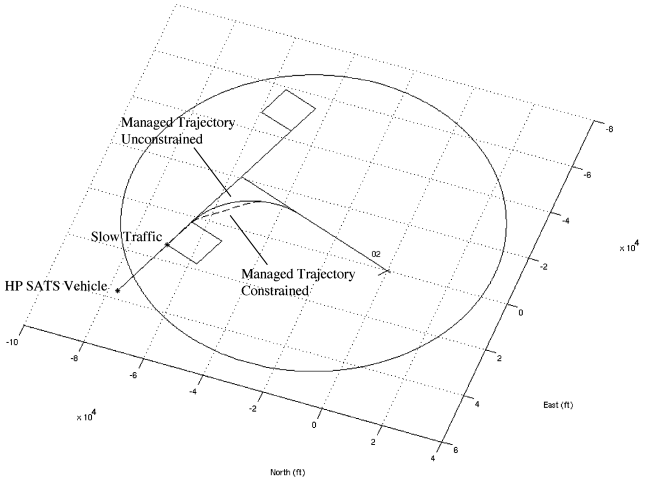

Fig. 15 Right-turn trajectory management; constrained case; top view.

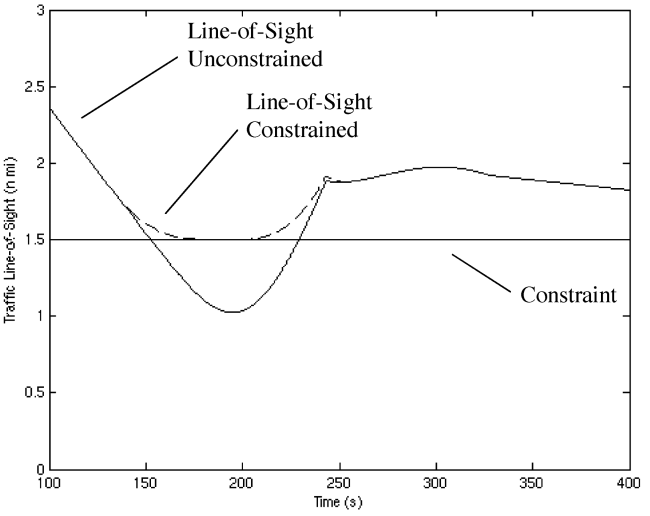

Fig. 16 Line-of-sight response; constrained case.

that HP SATS maintains the minimum allowable 1.5 n mile separation over the entire trajectory for enhanced safety.

C. Geometric State Control for Automatic Piloting

To demonstrate the managed geometric state trajectories in Sec. III.A can actually be performed by SATS aircraft; and, in particular, in autoflight mode, the descent profiles are simulated with nonlinear six degree-of-freedom closed-loop dynamics. A flight dynamic model of a generic advanced four-passenger private piston airframe commonly discussed in the SATS arena is considered. Vehicle characteristics are consistent with constant mass, rigid body modeling assumptions commonly applied in aircraft modeling and simulation [13]. Nonlinear table lookup aerodynamic and propulsive characteristics are also considered. Control inputs are available for guiding the vehicle include elevator Δ_E, aileron Δ_A, rudder Δ_R, throttle Δ_{Th}, and speed brake Δ_{SB}. A wide variety of output signals are available for feedback.

Attitude control and trajectory guidance systems are designed conventionally. Nonlinear vehicle dynamics are trimmed and linearized at the condition $H = 5000$ ft and $V = 190$ ft/s. Linear controllers for the longitudinal and lateral–directional dynamics are designed and then applied to the nonlinear dynamics. A fixed control parameter set is used during the descent profiles and does not require gain scheduling. Figures 17 and 18 show the linearized (lowercase variables) control diagrams. Inner-loop control architecture consists of speed command V_c and flight-path command Γ_c for longitudinal control, and heading command χ_c and yaw rate command R_c for lateral–directional control. Outer-loop trajectory management and guidance logic drive the inner loops with position–velocity commands X_c, Y_c, Z_c, $\dot{X}_c$, $\dot{Y}_c$, and $\dot{Z}_c$. Response outputs used for feedback include roll-pitch-yaw rates P, Q, R, roll-pitch angles Φ, Θ, heading χ, flight path Γ, speed V, and positions X, Y, and Z.

The following cases were generated with only heading, flight path, and speed commands (i.e., $K_s = 0$, $K_{d_V} = 0$, $K_{d_h} = 0$ where s denotes distance along the trajectory, $d_v - d_h$ denote vertical–horizontal displacements off the trajectory). Figures 19–24 show results for the nonlinear six degree-of-freedom closed-loop simulation corresponding to the unconstrained and constrained right-turn trajectory management cases in Figs. 11 and 13. The command curves denote the variable heading, flight path, and speed signals corresponding to the helical (combined circle and hyperbola) transition segments in Fig. 11 that were calibrated with Eqs. (21–23), as well as the distorted curve obtained from Eqs. (24–27) and displayed in Fig. 13. Because the constrained trajectory is a shorter path, and because the distorted path construction is such that the vehicle is time-synchronized to the unconstrained path at the initiation and termination distortion points and the minimum line-of-sight point, the vehicle modulates speed accordingly (see Fig. 24) during the altitude swell and S turn. The guidance system exhibits small tracking error and has no difficulty in executing the desired descent profiles. Feasibility of flying such time-efficient trajectories in the SATS environment are validated by the demonstrated tracking performance shown in Figs. 19–24.

IV. System Vision

Although well beyond the scope of this preliminary effort, description of a fully developed trajectory management guidance system (TMGS) applicable to future SATS concepts is provided here. A primary function of this envisioned TMGS is to provide flight management assistance and automation to exploit the SATS infrastructure, including high-performance vehicle capabilities and information-rich environments, while conducting ascent–descent transition between en route flight and runway threshold conditions coordinated with HVO operations. A secondary function of the envisioned TMGS is to provide operational safety by maintaining positive separation from traffic, weather, and airspace restrictions, as well as providing a degree of situational awareness of the surrounding airspace environment. TMGS should thus provide an effective balance between extracting flight performance and providing operational safety.

Figure 25 depicts an external architecture of the envisioned TMGS, emphasizing functionality and input–output data streams.

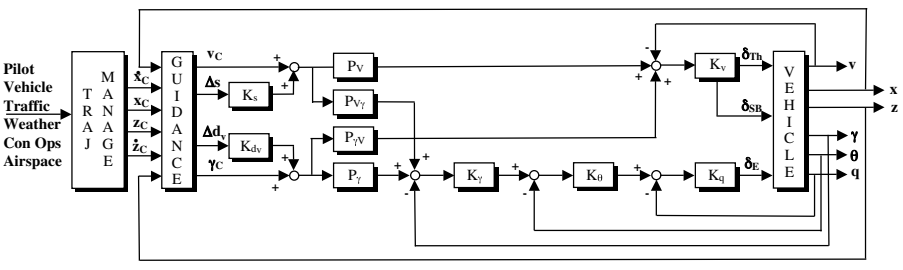

Fig. 17 Longitudinal autoflight control system.

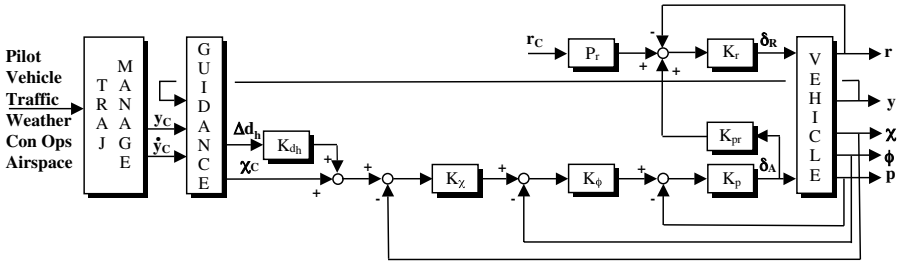

Fig. 18 Lateral–directional autoflight control system.

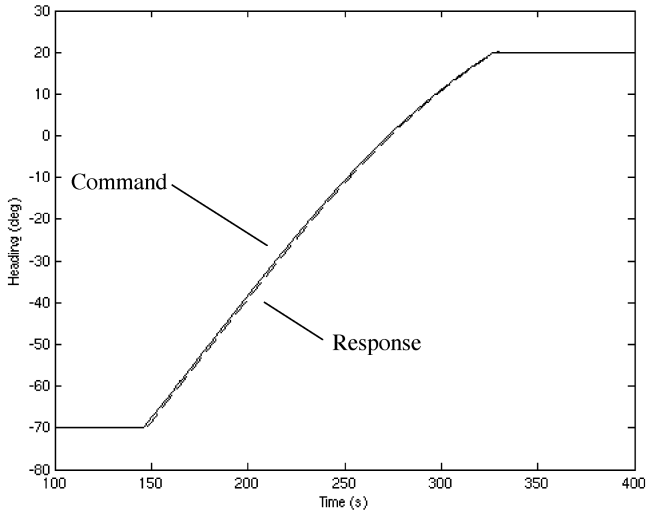

Fig. 19 Heading response; unconstrained case.

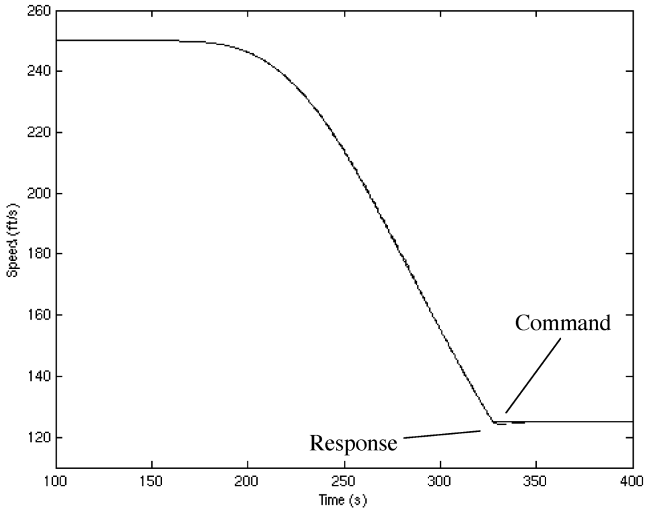

Fig. 21 Speed response; unconstrained case.

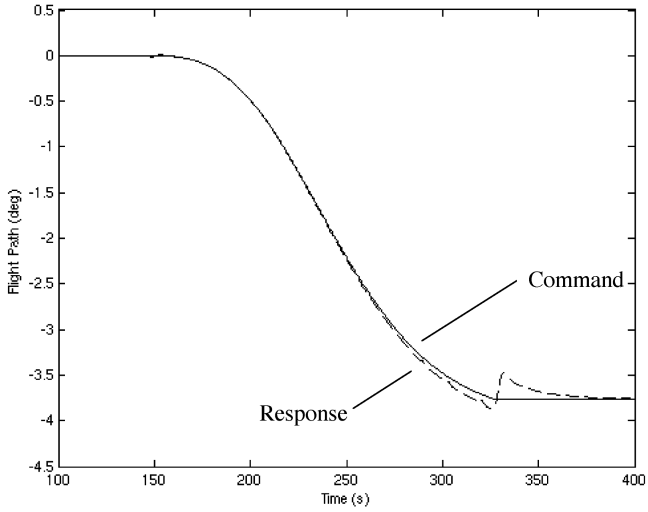

Fig. 20 Flight-path response; unconstrained case.

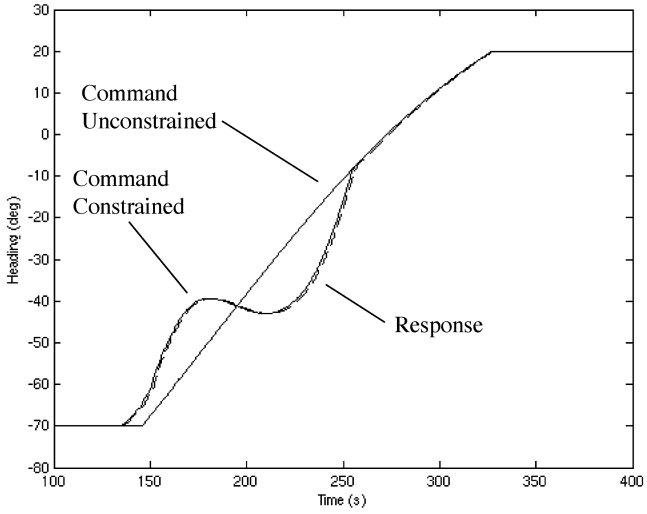

Fig. 22 Heading response; constrained case.

Preliminary internal capabilities were discussed in Secs. II and III. The system is primarily flight control logic implemented through software within the onboard flight management control system and cockpit architecture. Software logic shall be integrated with existing flight components such as inertial navigation system (INS) packages, global positioning system (GPS) receivers, primary flight and multifunction display (PFD/MFD) systems, and head-up display (HUD) units. In the near term, TMGS shall operate in a manual pilot mode by providing display commands for the human operator to follow. However, future enhancements shall provide an autopilot mode where commands are used to drive vehicle actuators in a closed-loop architecture. These modes are noted in Fig. 25.

As depicted in Fig. 25, input streams to the TMGS originate from various sources including SATS protocol, airspace topology, weather, traffic, vehicle-traffic model, sensor, and pilot. TMGS shall sample these information sources or communicate with sensors, receivers, and databases that provide such time-varying and time-invariant information. Governing SATS protocol (such as approach–departure geometry and associated HVO flight rules) and airspace topology data (including runway definition, obstacle warning, navigational restrictions, and noise procedures for individual airports) shall be available. Weather information shall include factors affecting flight performance and safety such as temperature, pressure, density, wind, precipitation, visibility, cloud state, turbulence, storm cells, etc. Traffic state data shall include aircraft identification and type, sequence assignment, HVO intent and conformance messages, and basic navigation information. Sensors shall provide an accurate description of the vehicle motion state.

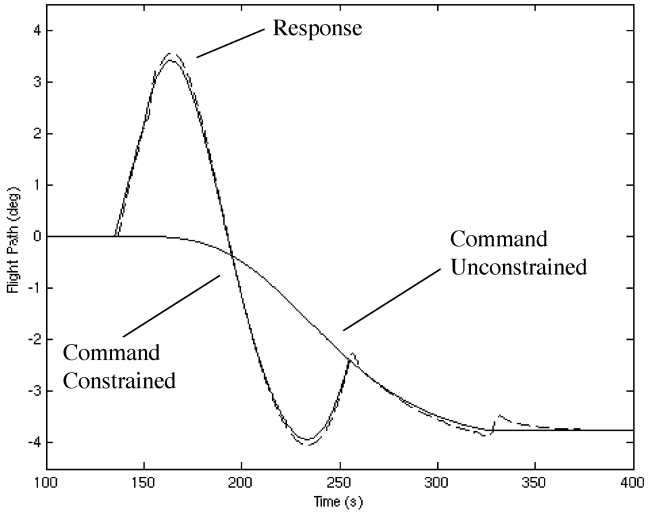

Fig. 23 Flight-path response; constrained case.

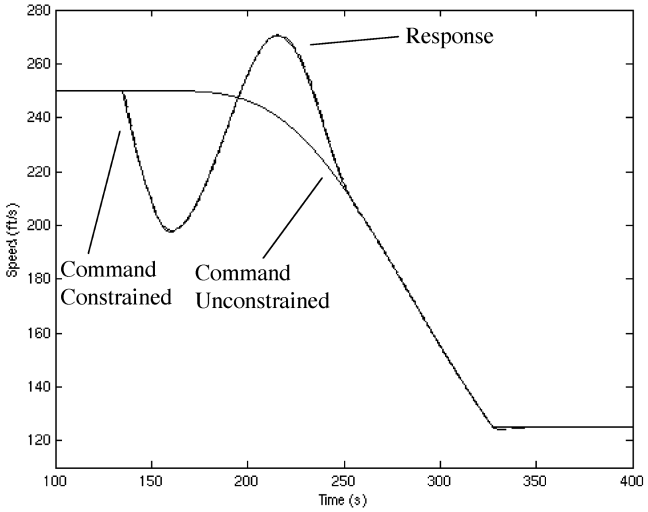

Fig. 24 Speed response; constrained case.

Vehicle and traffic models of the performance and flight dynamic types also shall be archived for use in the TMGS.

The pilot shall have options for selecting ascent–descent profile characteristics by designating various performance objectives. System functionality shall include performance options for flight time, fuel usage, noise abatement, ride comfort, workload ease, enhanced safety, and specified path. Depending upon factors such as schedule, fuel reserve, time of day, pilot fatigue level, etc., the pilot can emphasize various concerns. Further, operational constraints shall be activated, either explicitly or implicitly, through performance selections by the pilot. In certain cases, the pilot shall also input the numerical constraint value or desirable margin from the constraint boundary. Relevant constraints shall include limitations from a wide variety of factors such as HVO procedures, airspace geometry, terrain avoidance, weather evadence, traffic separation, vehicle performance, and human tolerance. Many of these constraints will require scheduling with flight phase, traffic type, and visibility–cloud state.

After accomplishing trajectory construction with constraint compliance, output streams from the TMGS are transferred to destinations denoted as display and actuator (see Fig. 25). The display shall illustrate the desired trajectory and energy–motion state information as visual numeric and geometric data to the pilot. Display data may consist of several or all of the following items: absolute desired position–velocity state, actual position–velocity state relative to the desired state, desired trajectory corridor, velocity vector cues, and spatial–temporal constraint boundaries and/or margins for traffic, terrain, and weather. Display information serves as manual commands for the pilot to implement, or as system status data for the pilot to monitor, during autopilot engagement. The actuator shall implement the commanded state, derived from the desired trajectory and energy–motion state information in the flight control system, by providing time–varying control input signals to the vehicle. Actuator signals may determine aerodynamic surface deflections, engine throttle and mixture settings, vehicle configuration states using high-lift devices or speed brakes, and mass centroid positioning by employing fuel distribution management. The autonomous commands from the autopilot are implemented by the actuator.

V. Conclusions

Methodology for construction and implementation of in-flight trajectory management systems for vehicles participating in future small aircraft transportation systems has been addressed. Adjustable approach paths between en route conditions and the terminal airspace boundary, based on energy state theory, demonstrated time-to-interface savings on the order of 10 min and can be used to circumvent slower traffic. Further, descent trajectories between the terminal airspace boundary and runway threshold, based on space–time curve theory, also demonstrated time-to-land savings on the order of 10 min by circumventing slower traffic. Additionally, line of

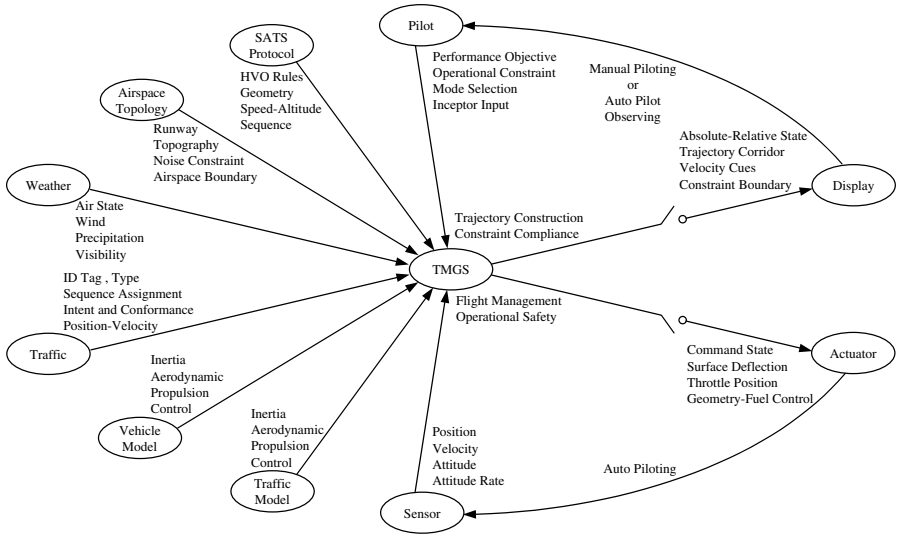

Fig. 25 External TMGS architecture.

sight to traffic constraints demonstrated that positive separations can be maintained while following the descent trajectories. These strategies contribute to the SATS air traffic management concept by facilitating additional airspace throughput efficiency and operational safety using the associated airborne and ground infrastructure technologies envisioned for SATS. Results imply that future, evolved HVO concept operations exhibiting increased efficiencies beyond current levels should be investigated.

Acknowledgments

This research was supported by NASA Langley Research Center, National Consortium for Aviation Mobility, and Virginia SATS Lab under the SATS program. Technical monitors included Sally Johnson, Fred Brooks, and Jon Paris. This support is appreciated.

References

[1] Holmes, B. J., Durham, M. H., and Tarry, S. E., "Small Aircraft Transportation System Concept and Technologies," *Journal of Aircraft*, Vol. 41, No. 1, 2004, pp. 26–35.

[2] Conway, S. R., and Consiglio, M., "A Method of Separation Assurance for Instrument Flight Procedures at Non-Radar Airports," AIAA Paper 2002-4448, 2002.

[3] Abbott, T. S., Jones, K. M., Consiglio, M. C., Williams, D. M., and Adams, C. A., "Small Aircraft Transportation System Higher Volume Operations Concept: Normal Operations," NASA CR-2004-213022, 2004.

[4] Baxley, B., Williams, D., Consiglio, M., Adams, C., and Abbott, T., "The Small Aircraft Transportation System, Higher Volume Operations Concept and Research Summary," AIAA Paper 2005-7379, 2005.

[5] Millsaps, G. D., "Small Aircraft Transportation System Simulation Analysis of the HVO and ERO Concepts," NASA CR-2003-212170, 2003.

[6] Bryson, A. E., Desai, M. N., Hoffman, W. C., "Energy-State Approximation in Performance Optimization of Supersonic Aircraft," *Journal of Aircraft*, Vol. 6, No. 6, 1969, pp. 481–488.

[7] Vinh, N. X., *Flight Mechanics of High-Performance Aircraft*, Cambridge Aerospace Series 4, Cambridge Univ. Press, Cambridge, England, U.K., 1993.

[8] Acheson, M. J., "Energy Based Method for Generation of Global Optimum Flight Path," M.S. Thesis, Dept. of Aerospace Engineering, Old Dominion Univ., Norfolk, VA, May 2006.

[9] Krizansky, M. G., "Three Dimensional Situational Awareness from Two Dimensional Displays and Simulation Techniques in Modern General Aviation Cockpits," M.S. Thesis, Dept. of Aerospace Engineering, Old Dominion Univ., Norfolk, VA, May 2006.

[10] Hildebrand, F. B., *Advanced Calculus for Applications*, Prentice-Hall, Englewood Cliffs, NJ, 1976.

[11] Leitmann, G. (ed.), *Optimization Techniques with Applications to Aerospace Systems*, Mathematics in Science and Engineering, Vol. 5, Academic Press, New York, 1963.

[12] Newman, B., Britcher, C., Kassaye, Y., Roy, J., Krizansky, M., and Acheson, M., "Trajectory Management Concepts for Future Small Aircraft Transportation Systems," *Digital Avionics Systems Conference (DASC 2005)* [CD ROM], Institute of Electrical and Electronics Engineers, Los Alamitos, CA, and AIAA, Reston, VA, 2005.

[13] Zipfel, P. H., *Modeling and Simulation of Aerospace Vehicle Dynamics*, AIAA Education Series, AIAA, Reston, VA, 2000.